Dalton Transactions

PAPER

View Article Online
View Journal | View Issue

Cite this: *Dalton Trans.*, 2014, **43**, 6897

Modulation of the electronic and spectroscopic properties of Zn(II) phthalocyanines by their substitution pattern

Sevinc Z. Topal,[a] Ümit İşci,[a] Ufuk Kumru,[a] Devrim Atilla,[a] Ayşe G. Gürek,[a] Catherine Hirel,[a] Mahmut Durmuş,[a] Jean-Bernard Tommasino,[b] Dominique Luneau,[b] Savas Berber,[c] Fabienne Dumoulin*[a] and Vefa Ahsen*[a]

Received 4th December 2013,
Accepted 4th February 2014

DOI: 10.1039/c3dt53410c

www.rsc.org/dalton

Four isomerically pure octasubstituted zinc phthalocyanines with variations in the attachment atom and positions of the substituents were selected for a systematic investigation of the effect of the substitution pattern on their electronic and spectroscopic properties. Effects which were investigated are the position, the electron donating and withdrawing properties, and the donating force of the substituent. The results are discussed and interpreted based on theoretical and experimental determination of the orbital levels. This work allows us to highlight which substitution patterns are the most suitable considering different common applications of phthalocyanines.

Introduction

Phthalocyanines – named in a more representative way tetrabenzotetraazaporphyrines, or tetrabenzoporphyrazines – are parent derivatives of porphyrins,[1] and remarkable molecular materials.[2] Most of their unique optical, spectroscopic, electronic and electrochemical properties come from their delocalized 18π electronic structure that can be tailored and tuned through structural modifications on the phthalocyanine macrocycle or at the metal center, as illustrated in Fig. 1. One possible structural modification is on the substitution pattern: the attachment atom, the hydrophilicity or hydrophobicity, the introduction of functional groups and the bulkiness of the substituents. The position, peripheral or non-peripheral, as well as the number of substituent are also to be considered. Tetrasubstituted phthalocyanines are obtained as regioisomeric mixtures. Only in some very rare cases the obtention of tetrasubstituted regioisomerically pure isomers has been reported, thanks to the bulkiness of the substituents[3] or on specific synthesis conditions.[4] On the contrary, octasubstituted phthalocyanines are isomerically pure.

The second type of possible structural variation is the metal center. Most of the metals or pseudo-metals ions have been inserted at the center of the macrocycle and as it may be expected they greatly affect the chemical and physical properties.[5] Moreover, for some metal ions, axial substitution is possible and may be used to introduce extra substituents.

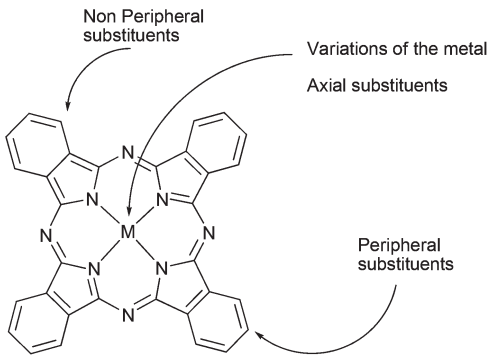

Fig. 1 The structural variations points on phthalocyanines. Inspired from ref. 6.

One of the main research focuses of our group is the design and preparation of photosensitisers for photodynamic therapy (PDT). So far, most of our efforts have been directed towards the preparation of water-soluble phthalocyanines derivatives introducing appropriate water-solubilizing substituents.[7] We also investigated the effect of metalation with different metal centers (Pt, Ga, In among others)[8] but Zn remains the most common, as it gathers several advantages, mainly its diamagnetism suitable for singlet oxygen generation thanks to richly populated triplet excited state. In addition, syntheses of Zn phthalocyanines are quite easy and high yielding. Zinc is there-

[a]*Gebze Institute of Technology, Faculty of Sciences, Department of Chemistry, 41400 Gebze, Kocaeli, Turkey. E-mail: fdumoulin@gyte.edu.tr, ahsen@gyte.edu.tr; Fax: +90 262 605 31 05; Tel: +90 614 262 605 30 22*
[b]*Université Claude Bernard Lyon 1, Laboratoire des Multimatériaux et Interfaces (UMR 5615), 69622 Villeurbanne cedex, France*
[c]*Gebze Institute of Technology, Faculty of Sciences, Department of Physics, 41400 Gebze, Kocaeli, Turkey*

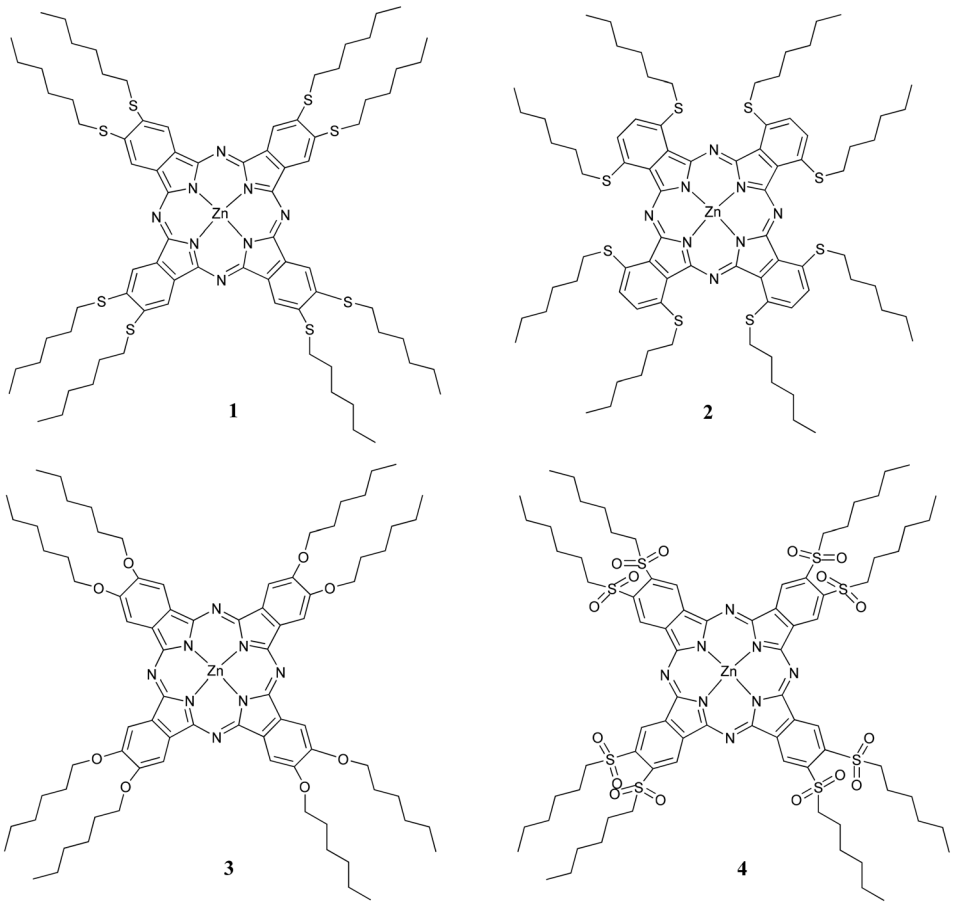

Fig. 2 Chemical structures of the zinc phthalocyanine derivatives **1–4**.

fore a metal of choice for properties mediated by an excited triplet state, such as the photodynamic generation of singlet oxygen and reactive oxygen species for PDT or photocatalysis.

At this point of our research, we felt the need for a fundamental and systematic study of how the substitution pattern of Zn phthalocyanines, and more specifically the attachment atoms and the position of the substituent, affect the photophysical, photochemical and electrochemical properties. The series of the four molecules which has been investigated in this study is represented in Fig. 2.

All molecules were designed in order to fulfill the following criteria:

- to be isomerically pure to avoid regioisomeric effects: octa-substitution pattern was selected;

- to have variations only at the attachment point: a hexyl chain is attached by a sulfur atom *via* a sulfanyl function in peripheral (**1**) and non-peripheral (**2**) position, or by an oxygen atom *via* an ether function (**3**) or by a sulfonyl function (**4**) in peripheral positions. The hexyl chain was chosen as it provides solubility in at least two common solvents for the planned measurements.

- to be in the monomeric state in selected solvents and prevent the aggregation which is likely to induce effects not related to the intrinsic structure of the molecules.

The investigated substitution pattern effects are:

- the substituent position (compounds **1**/**2**);

- the electron donating and withdrawing character (compound **1**/**4**);

- the donating force (compound **1**/**3**).

Having in mind a systematic investigation of the effect of these four different substitution pattern, we studied and compared for the four phthalocyanines **1–4** their electronic absorption and fluorescence spectroscopy, the singlet oxygen generation ability and their photostability, as well as their electrochemical behaviour. The results of the measurements were related to the orbital state of each phthalocyanine, which was determined from the experimental electrochemical studies and from theoretical orbital calculations.[9] These molecules are known, but are now grouped to form a series for the comparative purposes enounced above. If a very few data were available in the literature, all the measurements were completed by ourselves to avoid experimental artefact measurements.

Results and discussion

Along this work, all experimental studies of the physical properties were performed in solution. For the sake of measure-

ments, it was crucial that the four phthalocyanines were all in a non-aggregated monomeric state in one or two common solvents. Tetrahydrofuran (THF) and dichloromethane (DCM) were selected, taking into account the electronic absorption range of the molecules, and because the four phthalocyanines exhibited satisfying solubility in both solvents. Toluene, *N*,*N*′-dimethylformamide, dimethylsulfoxide, acetone or chloroform were tested and found to be inappropriate.

Ground state electronic absorption

Information available by looking at the ground state electronic absorption spectra of phthalocyanines is their maximum absorption wavelength, the extinction coefficient at these wavelengths, and the shape of the absorption bands which reflects the aggregation state. In particular, the position, intensity and sharpness of the Q band are determinant in most of phthalocyanines' applications. These parameters have been interpreted in close relation with the molecular structure of the four studied phthalocyanines. Besides, the position of the UV-vis absorption band edge (λ_{edge}) allows the calculation of the energy gap between the HOMO and LUMO levels for each derivative, as done later in the paper.

Ground-state absorption spectra of the zinc phthalocyanines were recorded in THF and DCM. Absorption maxima and extinction coefficients are presented in Table 1, and the UV-vis spectra are shown in Fig. 3. The colors of the four phthalocyanines in THF solution can be observed in Fig. 4. They exhibited typical electronic absorption spectra with a single intense $\pi\rightarrow\pi^*$ transition, referred to as the Q band, much intense and characteristic for phthalocyanines, and another less intense and broader $\pi\rightarrow\pi^*$ transition which is the so-called Soret band (B).

Sharp and single Q bands of compounds **1**, **3** and **4** are typical of non-aggregated monomeric phthalocyanines in both solvents. Phthalocyanine **2**, with a slightly broadened Q-band centred at 779 nm in THF can be considered as monomeric, but aggregated in DCM as evidenced by its broad, decreased and red-shifted Q band. Compared to THF, this Q band is red-shifted by 21 nm in DCM. According to Kasha's exciton theory,[10,11] it may imply that phthalocyanine **2** forms J aggregates in DCM. Non-ionic detergents such as Triton X-100 reverses aggregation processes, and indeed, the addition of Triton X-100 enhanced the sharpness of the Q band of **2**, confirming that its shape was due to aggregation (spectrum not represented).

These observations in both solvents (Table 1 and Fig. 3 and 4) show that the four phthalocyanines keep their Q band maxima in the same range, affected only by the variation of

Table 1 Absorption spectra related data of **1–4** in THF and DCM

Compound	Solvent	Q band λ_{max} (nm), (log ε)	Soret band λ_{max} (nm), (log ε)
1	THF	704 (5.47)	369 (4.97)
1	DCM	711 (5.06)	357 (4.94)
2	THF	779 (5.11)	354 (4.69)
2	DCM	800 (4.26)	355 (4.00)
2	DCM + Triton X-100	780 (5.12)	342 (4.59)
3	THF	672 (5.66)	359 (5.17)
3	DCM	678 (4.78)	345 (4.43)
4	THF	682 (5.47)	377 (4.77)
4	DCM	686 (5.48)	370 (4.86)

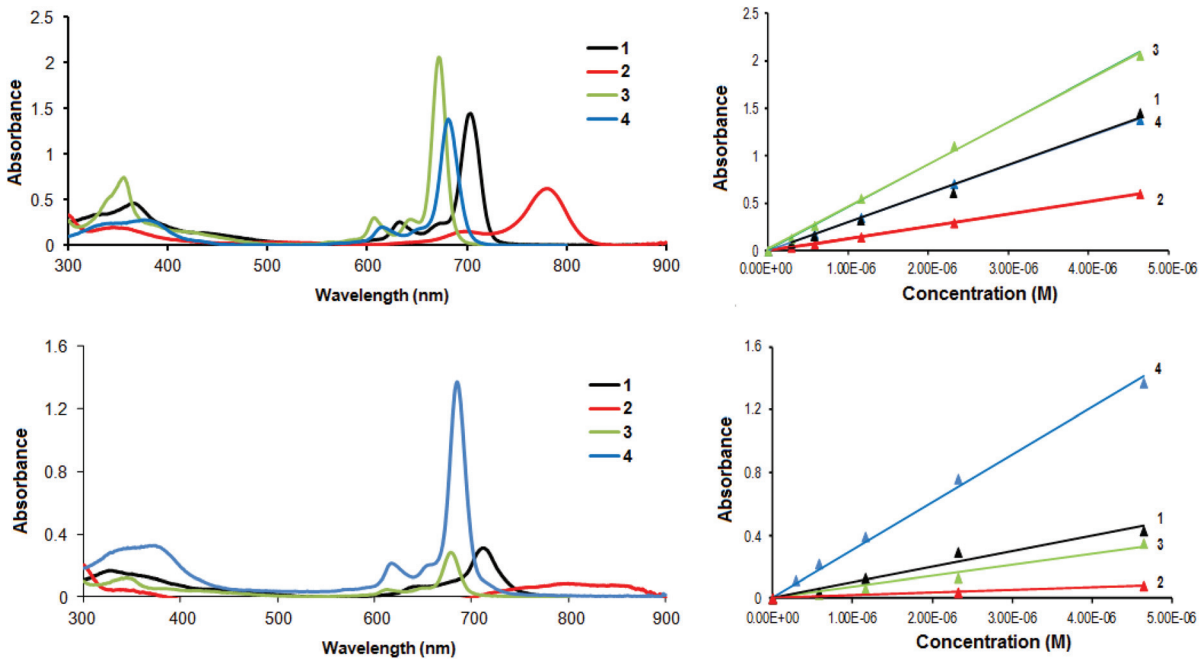

Fig. 3 Left hand side: UV-Vis spectra of **1**, **2**, **3** and **4** in THF (top) and in DCM (bottom) at the same concentration (~4.5 × 10^{-6} M). Right hand side: plots of Q band absorption intensities *vs.* concentration in THF (top) and in DCM (bottom).

Fig. 4 Solutions of phthalocyanines **1–4** in THF (~3 × 10^{-5} M).

the substitution pattern: $\lambda_{max(Q)}$ **2** > **1** > **4** > **3**. The presence of strong electron-donor groups, like in **1** relatively to **3** and **4**, and of non-peripheral position, like in **2** relatively to **1**, induces a red-shift of the Q band to longer wavelengths. These effects are actually known[12,13] and scholarly demonstrated in the present study, to be exploited in particular for application requiring NIR absorption.[14] The most dramatic effect is the substituent positions, as highlighted by the red-shift of the Q band of **2** compared to that of **1** by 75 nm in THF and 89 nm in DCM. The effect of the strength of the electron-donating nature is evidenced by looking at the Q band maxima of **3**. It is blue shifted by approximately 25–30 nm compared to **1**, due to the lower electron-donor effect of the oxygen atom compared to the sulfur atom attaching the hexyl chains. A comparison of the position of the Q band maximum of **1** and **4**, bearing respectively electron-donating and electron-withdrawing substituents, reveals that **4** exhibits a blue shifted Q band by 22–25 nm with respect to **1** in both solvents, due to the electron withdrawing nature of hexylsulfonyl groups in **4**. Finally, one can notice that **3** has the shortest Q band wavelength, revealing the relatively larger HOMO–LUMO gap of zinc phthalocyanine with oxygen attachment. These observations are in accordance with the energy levels of the frontier molecular orbitals determined either *via* electrochemical measurements or by theoretical calculations.

In addition to the position of the absorption, its intensity quantified by the molar extinction coefficient (ε) is determinant. The ε values were determined in both THF and DCM for the four phthalocyanines, by plotting the Q band absorption intensities *versus* (*vs.*) concentration (Fig. 3), and are typically high in both solvents. The linearity of the Lambert–Beer law is followed for the whole concentration measurement range.

Fluorescence properties

Steady-state fluorescence measurements. Fluorophores with excitation and emission at long wavelengths, in order to limit possible interferences with biological material absorbing at shorter wavelengths,[15] are decisive for biological applications such as imaging in PDT,[16] photodiagnostic[17] and live-cell fluorescence microscopy.[18] Zn(II) phthalocyanines are used as well as fluorescence-based sensors for metal detection[19] or pH variations.[20]

Fluorescence steady-state measurements provide information about the fluorescence excitation and emission wavelengths and intensities, the Stokes shifts and the fluorescence quantum yields. These data are presented in Table 2, together with photodynamic data commented later in the paper. Some fluorescence properties of **1** in THF and DCM were reported earlier by our group.[21]

Fluorescence excitation and emission maxima are all in the very NIR region. Fluorescence emission spectra of the four phthalocyanines were recorded in THF and DCM, upon excitation around 650 nm (Fig. 5). To calculate the fluorescence quantum yield, the fluorescence area integration of the four phthalocyanines *vs.* absorbance was plotted (Fig. 5), using the values of unsubstituted Zn(II) phthalocyanine in DMSO[22a] for **1**, **3** and **4**, and of unsubstituted Zn(II) naphthalocyanine for **2** in DMSO[22b] as well (see details in Experimental section). Compounds **1**, **3** and **4** have the highest and relatively similar fluorescence characteristics (Fig. 5), alike **2** which exhibits a larger Stokes shift and lower quantum yield and lifetime. This trend fits previous observations on the substituent position and nature effect.[13] The aggregation of **2** in DCM prevented the electronic events leading to fluorescence emission, through non-radiative dissipation of energy by the aggregates. To detect fluorescence, Triton X100 was then added to **2** in

Table 2 Fluorescence spectra related data of the compounds in THF and DCM (λ_{ex}^{em}: excitation wavelength used for emission, λ_{max}^{ex}: maximum excitation wavelength, λ_{max}^{em}: maximum emission wavelength, $\Delta\lambda_{ST}$: Stoke's shift, Φ_F: fluorescence quantum yield, τ_F: fluorescence lifetime, k_f; fluorescence rate constant, k_{nr}: non-radiative rate constant, Φ_Δ: singlet oxygen quantum yield and Φ_d : photodegradation quantum yield)

Compound	Solvent	λ_{ex}^{em} (nm)	λ_{max}^{em} (nm)	λ_{max}^{ex} (nm)	$\Delta\lambda_{ST}$ (nm)	Φ_F	τ_F (ns)	k_f (s^{-1}) (10^6)	k_{nr} (s^{-1}) (10^6)	Φ_Δ	Φ_d ($\times10^{-4}$)
1	THF	670	711	706	5	0.13	2.96	43.9	293.9	—	—
1	DCM	670	718	711	7	0.04	—	—	—	0.32	6.48
2	THF	700	809	786	23	0.01	1.17	8.6	846.1	—	—
2	DCM	710	796	782	14	0.02*	—	—	—	0.06	10.20
3	THF	640	676	672	4	0.19	3.75	50.7	216.0	—	—
3	DCM	650	685	679	6	0.09	—	—	—	0.52	83.60
4	THF	650	693	685	8	0.15	3.83	39.2	221.9	—	—
4	DCM	655	696	689	7	0.15	—	—	—	0.66	0.19

—: Not measured. *: presence of Triton X-100. $k_f = \Phi_F/\tau_F$. $k_{nr} = (1 - \Phi_F)/\tau_F$.

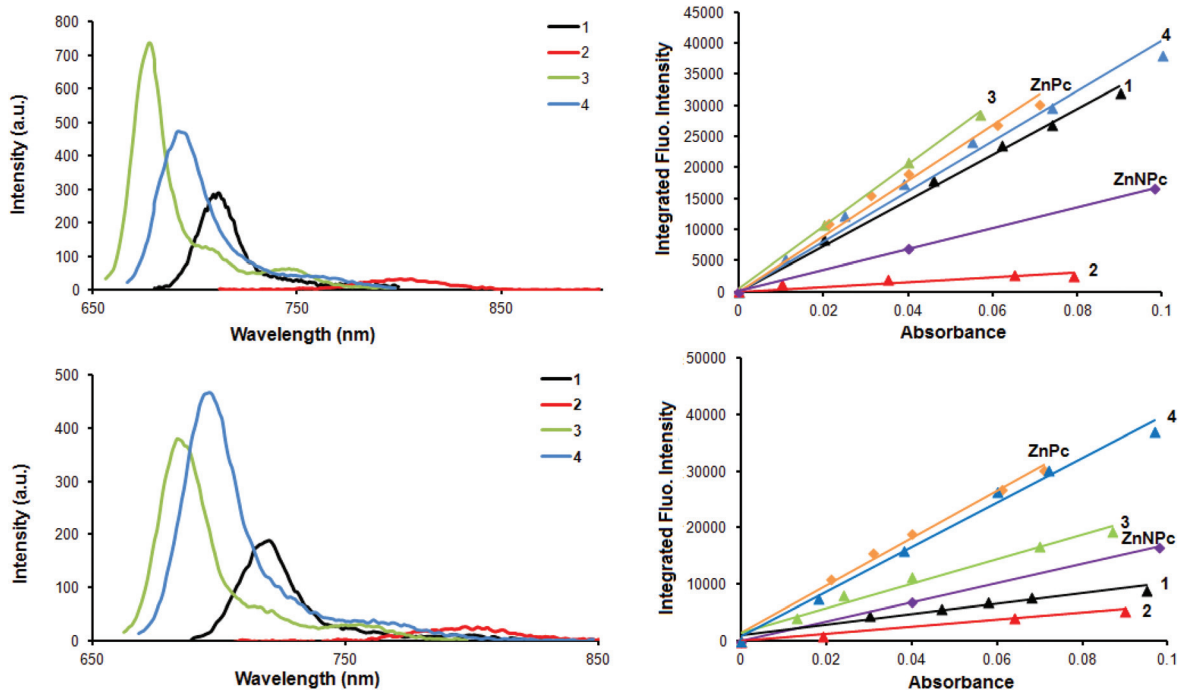

Fig. 5 Left hand side: fluorescence emission spectra of **1**, **2**, **3** and **4** in THF (top) and in DCM (bottom) (normalized for absorbance values ~0.04). Right hand side: integrated fluorescence area integration *vs.* absorbance in THF (top) and in DCM (bottom). For reference molecules (unsubstituted zinc phthalocyanine ZnPc and unsubstituted zinc naphthalocyanine ZnNPc), fluorescence area integration *vs.* absorbance in DMSO is added respectively in orange and in purple in both graphics.

DCM in order to inhibit aggregation as seen above. Peripherally hexylsulfanyl substituted phthalocyanine **1** shows a much higher Φ_F value compared to non-peripheral analogous phthalocyanine **2**. This is due to a lower quenching of the excited singlet state in peripherally substituted derivatives.[23]

Compounds **1**, **3** and **4** exhibit average Φ_F values in both solvents and small Stokes shifts (5–8 nm), which is a known characteristic of phthalocyanines.[19] When comparing the electron-donating force (**1** *vs.* **3**), an increase of Φ_F is observed for the lower electron-donating force. Substitution by electron-withdrawing hexylsulfonyl moieties enhances this effect: the highest Φ_F is observed for **4**.

The solvent itself affects the fluorescence quantum yields. Phthalocyanines **1**, **3** and **4** have their maximum of the excitation and emission wavelengths slightly red-shifted and their quantum yields lowered in DCM compared with THF, with **4** being the less affected.

Fluorescence lifetimes (time-resolved measurements). Fluorescence lifetime is quantified by time-resolved fluorescence measurements, and is an important parameter in applications such as fluorescence-based sensors,[24] molecular probing[25] and molecular imaging.[26] Fluorescence lifetime of each phthalocyanine was measured in ambient conditions in THF, the solvent in which compounds have the best quantum yields. Data are presented in Table 2, and time-resolved fluorescence profiles of each phthalocyanine are represented in Fig. 6. Phthalocyanines **2**, **3** and **4** exhibited single exponential decay when **1** showed a biexponential function that yielded fluorescence lifetime constants of 2.96 ± 0.01 ns (98.4%) and 124.19 ± 4.88 ns (1.6%). One can observe the following trend, from the shortest to the longest lifetime values: **2** < **1** < **3** < **4**. Fluorescence lifetime is maximum for **4** bearing electro-withdrawing substituents. Comparing the substituent position effect between **1** and **2**, the non-peripheral position induces significantly shorter lifetimes. Corresponding fluorescence rate constants ($k_f = \Phi_F/\tau_F$) and non-radiative rate constants ($k_{nr} = (1 - \Phi_F)/\tau_F$) were calculated from these lifetime data, and are shown in Table 2.

It appears that despite its attractive NIR fluorescence properties, substitution pattern of **2** may not be suitable for fluorescence-based applications, peripheral hexylsulfonyl substitution pattern of **4** being much more appropriate.

Photodynamic potential

A photodynamic process is the generation of singlet oxygen by a photosensitiser upon appropriate irradiation. Singlet oxygen generation is crucial in photocatalysis and photodynamic therapy. This powerful oxidant can induce cell death by damaging cell components in biomedical applications such as PDT, can decompose pollutants[27] or can be used as a synthetic oxidant in photocatalytic applications.[28] Depending on the targeted applications, various ranges of photostability of the photosensitiser are desired. It results of a three partner process: a photosensitiser, light and molecular oxygen. Singlet oxygen is generated by an energy exchange between a photosensitiser in its excited triplet state (^{3}PS*), relaxing to its

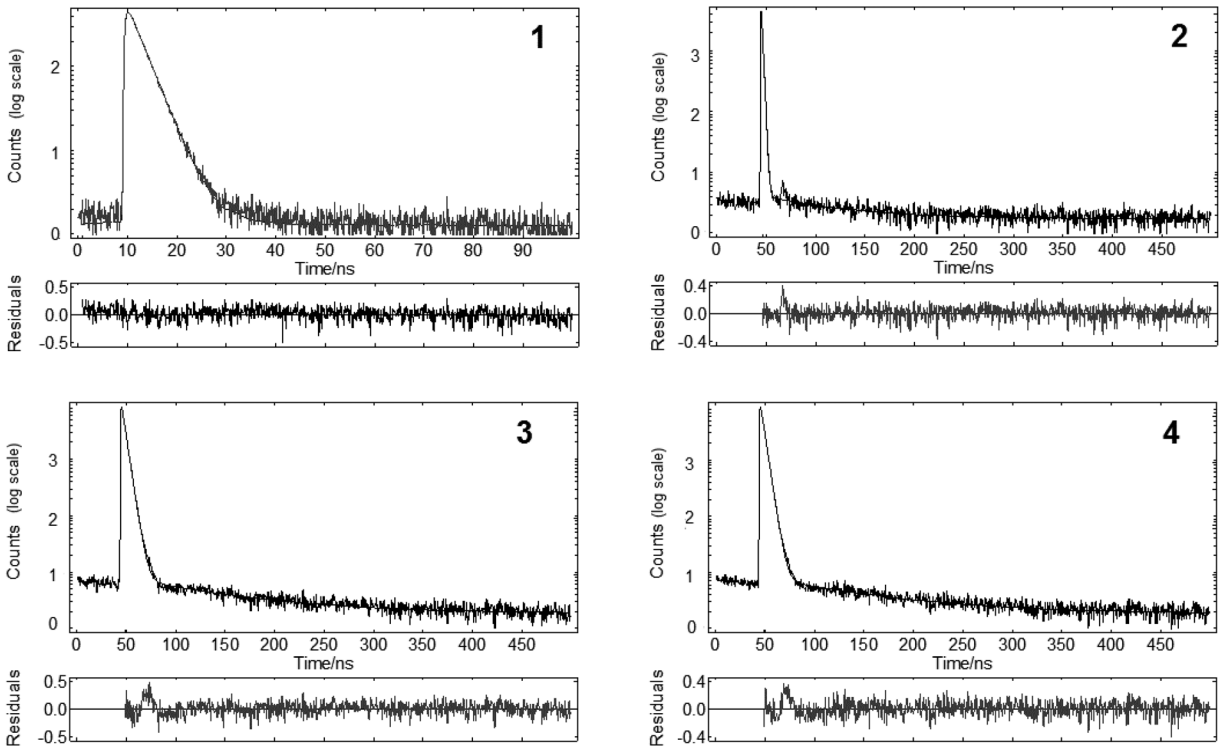

Fig. 6 Time resolved fluorescence decay profile for each phthalocyanine in THF (~1×10^{-6} M).

ground state by transferring energy to molecular oxygen.[29] The required energy to convert molecular oxygen to its singlet radical state is 0.98 eV,[30] and fits the energy gaps of phthalocyanines (see section on molecular orbital levels and energy gaps).

Singlet oxygen quantum yields. A good photosensitiser must exhibit high triplet lifetime and triplet quantum yield. Singlet oxygen quantum yield (Φ_Δ) is directly correlated to the photosensitiser's triplet quantum yield, and can be measured by optical, chemical and calorimetric methods. Optical determination of $^1O_2$ can be performed by two main methods: (1) direct monitoring of $^1O_2$ phosphorescence at 1270 nm,[31] (2) indirect measurements based on the use of a chemical quencher.[30] Herein, the direct detection of phosphorescence peak of $^1O_2$ at 1270 nm in DCM was monitored, and the corresponding singlet oxygen quantum yields (Φ_Δ) were calculated using phenalenone as a reference (Φ_Δ = 0.96 in DCM[32]) (Table 2). Singlet oxygen generation of **1**, **2**, **3**, **4** and phenalenone using the Stern–Volmer plot are presented in Fig. 7. For comparison purposes, the molecules were all excited at 365 nm, to use the same reference compound. Nevertheless, this does not reflect the potential of these phthalocyanines as NIR photosensitiser, but give the desired insights about the structural effects, which is the aim of this work.

Φ_Δ values are strongly affected by the substitution pattern and show the following trend: **2** < **1** < **3** < **4**, with respective values of 0.06, 0.32, 0.52, 0.66. The significantly higher Φ_Δ values are obtained for **3** and **4**, which are respectively the less electron-donating and electron-withdrawing members of the series, with an effect of the substitution pattern far more pronounced than reported for previous series.[26] In summary, singlet oxygen quantum yield decreases with the increase of donating properties of substituents, peripherally electron-withdrawing hexylsulfonyl substitution of **4** leading to higher $^1O_2$ production, reflecting an optimized triplet energy transfer from **4*** to molecular oxygen.

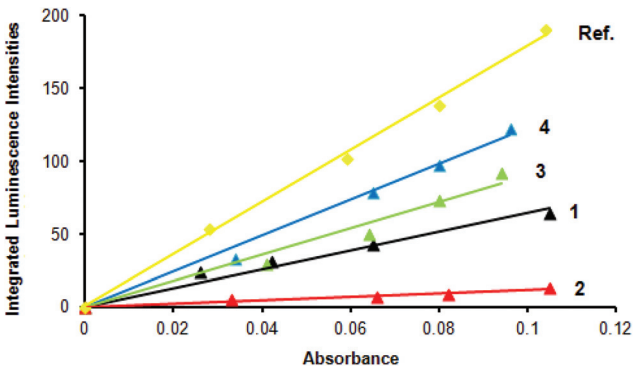

Fig. 7 Phosphorescence emission area integration (integrated luminescence intensities) of $^1O_2$ at 1270 nm *vs.* absorbance of **1**, **2**, **3**, **4** and reference phenalenone in DCM at 298 K. For all molecules, λ_{ex} = 365 nm.

Photostability. Depending on the targeted application, different ranges of photostability are desired. When photocatalysis requires a maximized photostability, biomedical applications appreciate lower photostability to assist the body

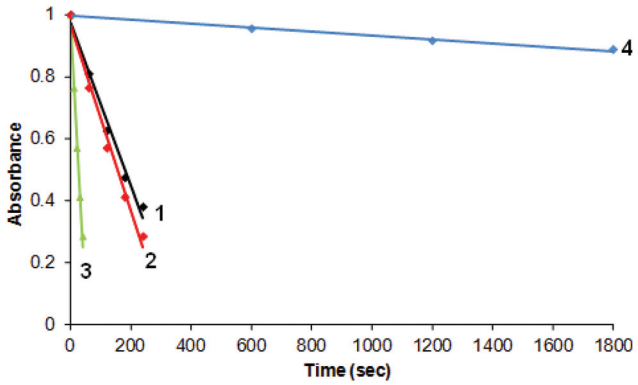

Fig. 8 Photodegradation profiles of compounds **1**–**4** in DCM (~4.5 × 10^{-6} M).

clearance of the photosensitiser. Photodegradation is the inverse parameter of photostability. The lowest is the photodegradation of a photosensitiser, the better is the photostability.

Photodegradation of the phthalocyanines was tested in DCM, the solvent used for singlet oxygen quantum yields determination. Photodegradation profiles are presented in Fig. 8, and the quantum yields are presented in Table 2, evidencing the uttermost photostability of **4**. As can be seen in Fig. 8, compounds **1**, **2** and **3** bleach much faster than **4**. Due to the electron-withdrawing effect of hexylsulfonyl groups[33] and its already chemically oxidized form, **4** is more difficult to oxidize and, therefore is highly photostable. As expected from these considerations, **4** exhibits the far best photostability corresponding to its very low photodegradation quantum yield.

Due to its efficient singlet oxygen generation and excellent photostability, peripheral hexylsulfonyl substitution pattern of **4** can be considered as the most suitable when designing photosensitisers for the photoproduction of singlet oxygen.

Electrochemical characterization

The electrochemical behaviour of the four phthalocyanines was investigated by cyclic voltammetry (CV) in dried THF containing 0.1 M tetra-(*n*-butyl)ammonium hexafluorophosphate (*n*-Bu_4NPF_6) as the supporting electrolyte. Phthalocyanine concentration was fixed at 5×10^{-4} M to avoid aggregation. DCM had to be used as well for **4** as its oxidation potential overlaps with THF oxidation. Recorded cyclic voltammograms (V *vs.* Ag/Ag^+) of **1**, **2**, **3**, **4** in THF and of **4** in DCM are shown in Fig. 9. All the processes are reversible or quasi-reversible. The ferrocenium/ferrocene

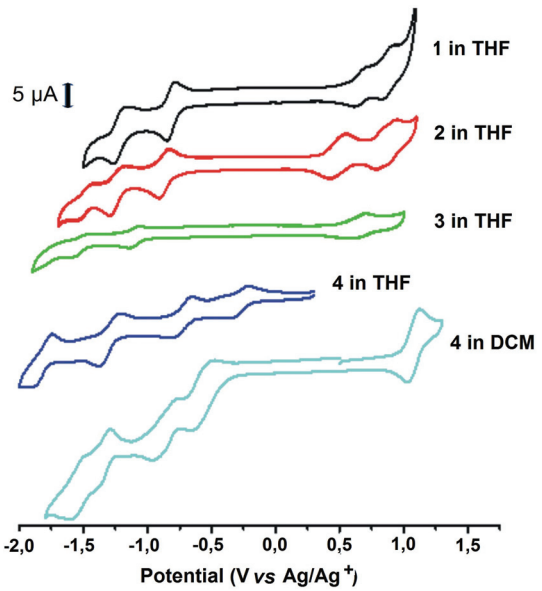

Fig. 9 Cyclic voltammetry profiles of ~5×10^{-4} M of **1**, **2**, **3**, **4** in THF and of **4** in DCM (0.1 mol dm^{-3} *n*-Bu_4NPF_6. Scan rate = 20 mV s^{-1}).

couple (Fc/Fc^+) was chosen as the internal standard reference. For comparison purposes, half-wave potentials ($E_{1/2}$) are given *vs.* (Fc/Fc^+), and are summarized in Table 3. A particular attention has been paid to the first oxidation and reduction potentials, as the difference between these two potentials corresponds to the HOMO–LUMO energy gap. This latter will be commented in the next section of the paper.

Since the central zinc cation is redox inactive,[34,35] all observed processes are attributed to successive removal/addition of electrons from/to the ligand-based orbitals. For all molecules, one electron exchange was involved in each of the oxidation and reduction steps. Generally, the peak currents of the processes exhibited a linear increase with the square root of scan rates ranging from 20 to 100 mV s^{-1}, indicating that the electrode reactions are diffusion-controlled.

Half-wave potentials ($E_{1/2}$) of **1** *vs.* Fc/Fc^+ obtained in THF are −1.37 V and −1.76 V in cathodic region, and +0.14 and +0.36 V in anodic region. These values are in accordance with previous reports in which **1** exhibited similar redox processes in DCM, with a small potential variation due to different experimental conditions regarding the reference electrode and supporting electrolyte used.[36,37]

Half-wave potentials ($E_{1/2}$) of **2** in THF *vs.* Fc/Fc^+ are −1.38, −1.77 and −2.01 V in the cathodic region, −0.03 and +0.28 V

Table 3 Half-wave redox potentials of the compounds (V) *vs.* Fc/Fc^+ couple

Compound	Solvent	Oxd_2	Oxd_1	Red_1	Red_2	Red_3	Red_4
1	THF	+0.36	+0.14	−1.37	−1.76	—	—
2	THF	+0.28	−0.03	−1.38	−1.77	−2.01	—
3	THF	—	+0.15	−1.59	−2.01	—	—
4	THF	—	—	−0.68	−1.13	−1.68	−2.22
4	DCM	—	+0.88	−0.74	−1.05	−1.61	−1.75

in the anodic region. Compared to **1**, and in accordance with reported data,[38] **2** exhibited shifts to negative potentials, for all processes and in particular for all oxidation peaks (Fig. 9):[36] **2** oxidizes more easily than **1**, and is slightly more difficult to reduce than **1**. The energy level of the HOMO orbital seems affected by the position of the substituent. The non-peripheral position has a stronger donor effect than can be correlated to its easier oxidation and its red-shifted absorption. Half-wave potential difference ($\Delta E_{1/2} = |E_{1/2}(\mathrm{ox}_1) - E_{1/2}(\mathrm{red}_1)|$) of **1** and **2** were found as 1.51 V and 1.35 V in THF, respectively. Relatively low half-wave potential difference for **2** can be attributed to the red-shifted absorption (75 nm) between **1** and **2**.

Half-wave potentials ($E_{1/2}$) of **3** in THF *vs.* Fc/Fc^+ are −1.59 and −2.01 V in the cathodic region and +0.15 V in the anodic region. Compared to **1**, this means that the energy level of the LUMO orbital seems largely affected in **3**. This indicates that the lower electron-donating character of **3** shifts the potentials. This is in accordance with literature information on the stronger donating effect of hexylsulfanyl phthalocyanine substitution compared to alkoxy substitution.[39,40] In addition, the larger potential difference between first reduction and first oxidation of **3** (1.74 V) compared with that of **1** (1.51 V) is in good agreement with the blue shift (32 nm) of the Q absorption band of **3** relative to **1**.

In THF, **4** *vs.* Fc/Fc^+ exhibited four cathodic peaks at −0.68 V, −1.13 V, −1.68 V and −2.22 V. However, its first oxidation peak could not be determined due to the narrow electrochemical window of THF, oxidation of the solvent beginning nearly after +1.0 V. Therefore, electrochemical measurements of **4** were also performed in DCM, yielding one anodic peak and four cathodic peaks (Fig. 9). The oxidation and reduction values are in accordance with previous reports, the small variation values being due to the different experimental conditions.[37] When strong electron-donating substituents decrease the oxidation potential, electron-withdrawing groups have the opposite effect, as evidenced earlier for zinc phthalocyanines[37] and free-based phthalocyanines.[36,41,42] In our case, the same trend was observed. The first reduction potential of **4**, which provides information about the LUMO level, is shifted by approximately ~0.7 V *vs.* **1**, in accordance with the study by Tylleman and coworkers.[42] In addition, larger half-wave potential difference of **4** (1.62 V) was for **1**, corresponding to the blue shift of 25 nm for the Q absorption band of **4**.

Molecular orbital levels and energy gaps

Molecular orbital energy levels and HOMO–LUMO energy gaps give precious information on the potentiality of a given compound for many applications. For example, it is widely used to estimate the potential of a dye-sensitized solar cell photosensitiser.[31,43,44] Along our study, calculations of the molecular orbital energy levels and of the energy gaps were performed to quantify the effects of substituent pattern. Molecular orbital energy levels can be determined from electrochemical measurements or by theoretical calculations. The band gap energy values that define the energy necessary for the transition of an electron from the HOMO to the LUMO level can be deduced from these data or obtained from the UV-vis absorption band edge (λ_{edge}). In the present work, the three methods were used to estimate these values which are summarized in Table 4.

Electrochemical determination. HOMO and LUMO energy levels of the compounds were calculated using the HOMO level of ferrocene at −4.8 eV[45] and the first oxidation and first reduction values of **1**, **2**, **3** in THF, and of **4** in DCM (Table 4). In this latest case and as mentioned above, measurements of **4** could be completed only in DCM, its first oxidation peak overlaps with THF oxidation itself. Eqn (1) and (2) were used for the calculation of HOMO and LUMO energy levels, respectively.

$$E_{\mathrm{HOMO}} = -[(E_{\mathrm{ox}} - E_{1/2(\mathrm{ferrocene})}) + 4.8] \quad (1)$$

$$E_{\mathrm{LUMO}} = -[(E_{\mathrm{red}} - E_{1/2(\mathrm{ferrocene})}) + 4.8] \quad (2)$$

Theoretical DFT calculations. Molecular orbitals and energy levels were also calculated theoretically, focusing on the geometries and electronic structures of the four phthalocyanines and using the generalized gradient approximation (GGA) to density functional theory (DFT) as implemented in the SIESTA code. The calculated energy levels of their frontier orbitals are shown schematically in Fig. 10 as 3D iso-density contour plots. The HOMO orbitals for **1**, **3** and **4** are centered on the phthalocyanine core, whereas in **2** the HOMO orbital has substantial contribution from the grafting sulfur atoms. Since the sulfur atoms in **2** are at a proper distance for an anti-bonding interaction, the HOMO level of **2** is shifted upward, and thus the energy gap is reduced.

The LUMO levels in Fig. 10 are double degenerate with only one of the states shown for each system. Theoretical values for

Table 4 HOMO and LUMO energy level values determined from experimental cyclic voltammetry (cv) and theoretical calculations (th), and band gap energy values found from UV-vis measurements

Determination methods	Electrochemistry			Theoretical (solvent free calculations)			From UV-vis absorption band edge
Compound (solvent)	$HOMO_{cv}$ (eV)	$LUMO_{cv}$ (eV)	E_g^{cv} (eV)	$HOMO_{th}$ (eV)	$LUMO_{th}$ (eV)	E_g^{th} (eV)	E_g^{opt} (eV)
1 (THF)	−4.94	−3.43	1.51	−4.59	−3.29	1.30	1.69
2 (THF)	−4.77	−3.42	1.35	−4.30	−3.34	0.96	1.49
3 (THF)	−4.95	−3.21	1.74	−4.54	−3.13	1.41	1.77
4 (DCM)	−5.68	−4.06	1.62	−6.22	−4.84	1.38	1.67

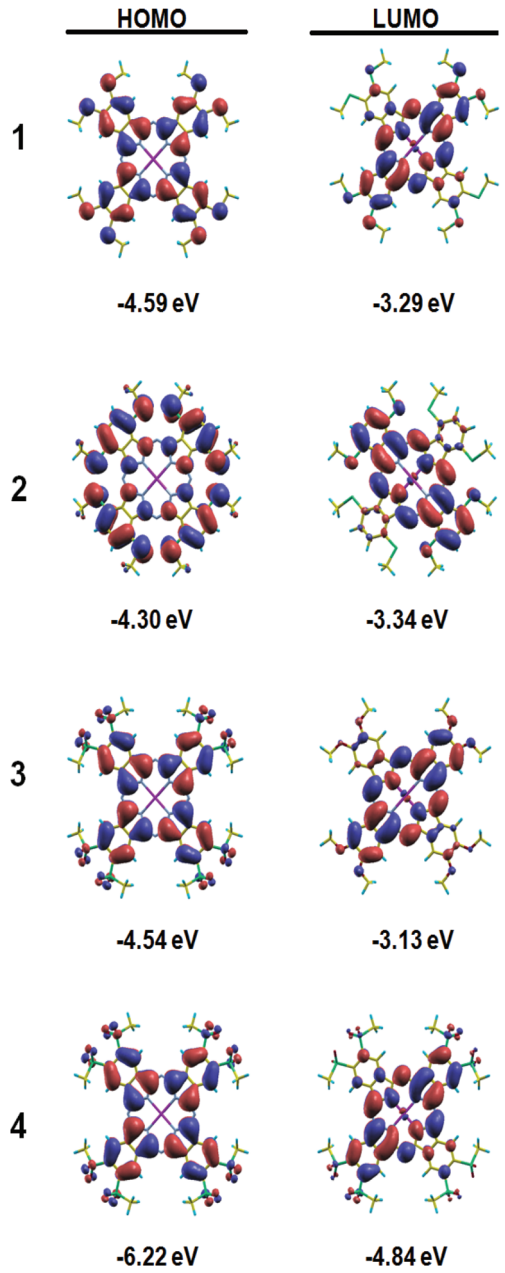

Fig. 10 Energies and isodensity representations of HOMO and LUMO orbitals calculated for **1**, **2**, **3** and **4**.

the LUMO level of the zinc phthalocyanines are very close to the experimental values determined from the CV measurements, except for **4**. As expected from a density functional theory calculation, the energy gaps are somewhat underestimated in our theoretical results.

Energy gap determination from UV-vis absorption band edge. Electronic UV-vis absorption is one of the most important properties of these molecules. The band gap can be obtained from the UV-vis absorption band edge (λ_{edge}) using eqn (3):

$$E_g^{opt}\ (eV) = 1240/\lambda_{edge}\ (nm) \quad (3)$$

where E_g^{opt} is the optical band and the number 1240 is obtained from the relationship between frequency and wavelength as described following eqn (4):

$$E(eV) = h\nu = h\frac{c}{e\lambda} \quad (4)$$

In this study, the values of the band gap energy (E_g^{cv}) found from cyclic voltammetry were in accordance with the values found from absorption band edge in UV-visible spectra (E_g^{opt}) (Table 4), and in agreement with earlier reports.[46]

Similar studies on porphyrins, which are tetrapyrrolic derivatives related to phthalocyanines, have demonstrated that incorporating electron-donating group on the porphyrin core results in decreased HOMO–LUMO energy gap, due to the considerable electronic coupling between the donor part and the porphyrin core.[41] This is consistent with our results reported here.

Conclusion

By selecting a series of four regioisomerically pure Zn(II) phthalocyanines with different substitution patterns, we completed experimentally systematic investigations of their photophysical, photochemical and electrochemical properties. These observations were related to their molecular orbital levels and HOMO–LUMO energy gaps. All data are in agreement with each other. Depending on targeted applications, the most suitable substitution patterns were identified, and two substitutions patterns could be distinguished: the octa non-peripheral hexylsulfanyl substitution pattern of **2** resulted in a remarkably red-shifted absorption appropriate for NIR absorption based applications; phthalocyanine **4** bearing hexylsulfonyl substituents exhibits unique photostability and singlet oxygen generation properties highly suitable for photodynamic applications.

Experimental

Synthesis

The synthesis of the four phthalocyanines **1**,[47] **2**,[48,49] **3**[50] and **4**[35] of this study has been previously reported and was performed according to reported procedures.

Solvents and reagents

All solvents and reagents were of reagent grade quality, and obtained commercially from Aldrich, Fluka or Merck. Dry solvents were obtained from a solvent purification system or from standard distillation methods unless otherwise noted. Triton X-100 and tetra(*n*-butyl)ammonium hexafluorophosphate (*n*-Bu_4NPF_6) were purchased from Aldrich.

Spectroscopic measurements

Absorption and steady-state fluorescence spectra were recorded using Shimadzu 2101 UV-Visible spectrophotometer and Varian Cary Eclipse spectrofluorometer, respectively.

Fluorescence lifetime measurements. Fluorescence lifetimes were recorded using a Time Correlated Single Photon Counting (TCSPC) system that was from Edinburgh Instruments (UK). The instrument was equipped with a 634.4 nm picoseconds pulsed LED as the excitation source (pulse width 79.3 ps) in the MCS mode. During measurements, the Instrument Response Function (IRF) was obtained from a non-fluorescence suspension of a colloidal silica (LUDOX 30%, Sigma Aldrich) in water, held in 10 mm path length quartz cell and was considered to be wavelength independent. All lifetimes were fit to a χ^2 value of less than 1.1 and with residuals trace symmetrically distributed around the zero axes.

Fluorescence quantum yield determination. Fluorescence quantum yield values (ϕ_F) were calculated employing the comparative William's method.[51] For this purpose, the absorbance and emission spectra of a reference standard and phthalocyanine compounds were measured at five different concentrations under identical conditions. The integrated fluorescence intensities were plotted *vs.* absorbance for reference and investigated phthalocyanines. The ratio of the gradients of the plots is proportional to the quantum yield. Unsubstituted zinc phthalocyanine was used as reference standard for **1**, **3** and **4**, its fluorescence quantum yield is 0.18 in DMSO.[22a,52] Unsubstituted zinc naphthalocyanine ZnNPc was used a reference standard for **2**, its fluorescence quantum yield is 0.07 in DMSO.[22b] Quantum yield (ϕ_F) values were calculated according to eqn (5) where ST and X designate standard and sample, respectively. Grad is the gradient of the plot and n is the refractive index of the solvent.

$$\phi_F = \phi_{ST}\left(\frac{\mathrm{Grad_X}}{\mathrm{Grad_{ST}}}\right)\left(\frac{{n_x}^2}{{n_{ST}}^2}\right) \quad (5)$$

Singlet oxygen yield determination. For singlet oxygen phosphorescence measurements, Horiba-Jobin Yvon Fluorolog-3R spectrofluorimeter with liquid nitrogen cooled, solid indium/gallium/arsenic detector (850–1600 nm) was used. Singlet oxygen productions were measured in DCM by optical method based on the comparison of singlet molecular oxygen phosphorescence in the near infrared region at 1270 nm produced by the phthalocyanines with singlet molecular oxygen phosphorescence produced by the reference sensitizer (phenalenone) in DCM (Φ_Δ value is 0.96 in DCM).[32] The absorbance of the studied phthalocyanine and of phenalenone at five different concentrations was recorded. The phosphorescence of the produced singlet oxygen generated was measured for each concentration. The resulting singlet oxygen integrated phosphorescence intensities were plotted *vs.* the absorbance of the studied phthalocyanine and of phenalenone. The ratio of the gradients of the plots was proportional to the singlet oxygen quantum yield (Φ_Δ), calculated according to eqn (6).

$$\phi_\Delta = \phi_{ST}\left(\frac{\mathrm{Grad_X}}{\mathrm{Grad_{ST}}}\right) \quad (6)$$

Photodegradation quantum yield determination. Photodegradation quantum yields were determined using eqn (7),

$$\Phi_d = \frac{(C_0 - C_t)VN_A}{I_{abs}St} \quad (7)$$

where C_0 and C_t are the samples' concentrations before and after irradiation respectively, V is the reaction volume, N_A: Avogadro's constant, S: irradiated cell area and t: irradiation time. I_{abs} is the overlap integral of the radiation source light intensity and the absorption of the samples. A light intensity of 3.09×10^{16} photons s^{-1} cm^{-2} was employed for photodegradation quantum yield (Φ_d) determinations.

Electrochemical measurements

Electrochemical measurements were performed by using an EG & G-Princeton Applied Research 263A all-in one potentiostat by using three-electrode setup with a glassy carbon working disk electrode (diameter: 3 mm) and a platinum wire auxiliary electrode. In order to avoid the problem of liquid junction potential, a silver wire (Ag/Ag^+ system) was used as pseudo-reference electrode. Tetra(*n*-butyl)ammonium hexafluorophosphate (n-Bu_4NPF_6) was used as supporting electrolyte (0.1 M). The ferrocenium/ferrocene couple (Fc/Fc^+) chosen as internal standard reference was added at the end of the experiment in all the experiments. The solutions were degassed with nitrogen gas and keep under this atmosphere during the electrochemical measurements. Positive feedback was used to IR Drop compensation. For the reversible or quasi-reversible systems, the half wave potentials; $E_{1/2}$ were calculated by the sum of $E_{p\,ox}$ (oxidation peak potential) + $E_{p\,red}$ (reduction peak potential) divided by 2.

Theoretical orbital calculations

In our atomic structure optimization and electronic structure calculations, we used the generalized gradient approximation (GGA) to density functional theory (DFT) as implemented in the SIESTA code.[53] We utilized Perdew–Burke–Ernzerhof[54] form of the exchange-correlation functional, norm-conserving Troullier–Martins pseudopotentials[55] with partial core corrections in the Kleinman–Bylander fully separable form,[56] and a double-ζ basis set augmented by polarization orbitals. The charge density and potentials were expressed on a real-space grid with a mesh cutoff energy of 200 Ry. The structure relaxations in conjugate-gradient algorithm were continued until all force components are less than 0.01 eV $Å^{-1}$. The fundamental energy gap for the fully relaxed structures were calculated as the difference between HOMO and LUMO levels. In order to lower the calculations time, all the structures were calculated with methyl groups instead of hexyl chains.

Acknowledgements

The authors thank gratefully Dr Yann Bretonnière for his assistance with the singlet oxygen quantum yields measurements. S. Z. T. thanks the French Embassy in Turkey for travel fellowships.

References

1 K. M. Kadish, K. M. Smith and R. Guilard, *Handbook of Porphyrin Science*, World Scientific, Singapore, 2012.
2 (*a*) C. G. Claessens, U. Hann and T. Torres, *Chem. Rec.*, 2008, **8**, 75; (*b*) J. Garcia, A. Gonzalez, A. Gouloumis, E. M. Maya, M. D. Perez, B. D. Rey, P. Vazquez and T. Torres, *Turk. J. Chem.*, 1998, **22**, 23; (*c*) P. Gregory, *J. Porphyrins Phthalocyanines*, 2000, **4**, 432.
3 J. Ranta, T. Kumpulainen, H. Lemmetyinen and A. Efimov, *J. Org. Chem.*, 2010, **75**, 5178.
4 S. Gaspard and P. Maillard, *Tetrahedron*, 1987, **43**, 1083.
5 C. G. Claessens, M. Cook, M. Hanack, R. J. M. Nolte, T. Torres and D. Wöhrle, *Monatsh. Chem.*, 2001, **132**, 3.
6 F. Dumoulin, M. Durmuş, V. Ahsen and T. Nyokong, *Coord. Chem. Rev.*, 2010, **254**, 2792.
7 (*a*) S. Tuncel, F. Dumoulin, J. Gailer, M. Sooriyaarachchi, D. Atilla, M. Durmuş, D. Bouchu, H. Savoie, R. W. Boyle and V. Ahsen, *Dalton Trans.*, 2011, **40**, 4067; (*b*) D. Lafont, Y. Zorlu, H. Savoie, F. Albrieux, V. Ahsen, R. W. Boyle and F. Dumoulin, *Photodiagn. Photodyn. Ther.*, 2013, **10**, 252.
8 (*a*) Y. Zorlu, F. Dumoulin, M. Durmuş and V. Ahsen, *Tetrahedron*, 2010, **66**, 3248; (*b*) V. Chauke, M. Durmuş and T. Nyokong, *J. Photochem. Photobiol., A*, 2007, **192**, 179.
9 G. D. Mori, Z. Fu, E. Viola, X. Cai, C. Ercolani, M. P. Donzello and K. M. Kadish, *Inorg. Chem.*, 2011, **50**, 8225.
10 M. Kasha, *Radiat. Res.*, 1963, **20**, 55.
11 M. Kasha, H. R. Rawls and M. A. EI-Bayoumi, *Pure Appl. Chem.*, 1965, **11**, 371.
12 T. Nyokong, *Coord. Chem. Rev.*, 2007, **251**, 1707.
13 N. Kobayashi, H. Ogata, N. Nonaka and E. A. Luk'yanets, *Chem.–Eur. J.*, 2003, **9**, 5123.
14 V. J. Pansare, S. Hejazi, W. J. Faenza and R. K. Prud'homme, *Chem. Mater.*, 2012, **24**, 812.
15 M. S. T. Gonçalves, *Chem. Rev.*, 2009, **109**, 190.
16 S. K. Pandey, A. L. Gryshuk, M. Sajjad, X. Zheng, Y. Chen, M. M. Abouzeid, J. Morgan, I. Charamisinau, H. A. Nabi, A. Oseroff and R. K. Pandey, *J. Med. Chem.*, 2005, **48**, 6286.
17 C. J. Kelty, N. J. Brown, M. W. R. Reed and R. Ackroyd, *Photochem. Photobiol. Sci.*, 2002, **1**, 158.
18 J. P. Celli, B. Q. Spring, I. Rizvi, C. L. Evans, K. S. Samkoe, S. Verma, B. W. Pogue and T. Hasan, *Chem. Rev.*, 2010, **110**, 2795.
19 S. Z. Topal, A. G. Gürek, K. Ertekin, D. Atilla, B. Yenigul and V. Ahsen, *Sens. Lett.*, 2010, **8**, 336.
20 (*a*) S. Z. Topal, E. Önal, A. G. Gürek and C. Hirel, *Dalton Trans.*, 2013, **42**, 11528; (*b*) S. Z. Topal, F. Yuksel, A. G. Gürek, K. Ertekin, B. Yenigul and V. Ahsen, *J. Photochem. Photobiol., A*, 2009, **202**, 205.
21 S. Z. Topal, A. G. Gürek, K. Ertekin, D. Atilla, B. Yenigul and V. Ahsen, *Mater. Chem. Phys.*, 2010, **121**, 425.
22 (*a*) I. Gürol, M. Durmuş, V. Ahsen and T. Nyokong, *Dalton Trans.*, 2007, 3782; (*b*) A. Ogunsipe, J. Y. Chen and T. Nyokong, *New J. Chem.*, 2004, **28**, 822.
23 M. Durmuş and T. Nyokong, *Tetrahedron*, 2007, **63**, 1385.
24 S. Borisov, K. Gatterer and I. Klimant, *Analyst*, 2010, **135**, 1711.
25 M. Y. Berezin, W. J. Akers, K. Guo, G. M. Fischer, E. Daltrozzo, A. Zumbusch and S. Achilefu, *Biophys. J.*, 2009, **97**, L22.
26 D. Álvarez, P. Medina and M. Moscoso, *Opt. Express*, 2009, **17**, 8843.
27 H. Kim, W. Kim, Y. Mackeyev, G. S. Lee, H. J. Kim, T. Tachikawa, S. Hong, S. Lee, J. Kim, L. J. Wilson, T. Majima, P. J. Alvarez, W. Choi and J. Lee, *Environ. Sci. Technol.*, 2012, **46**, 9606.
28 W. Spiller, H. Kliesch, D. Wöhrle, S. Hackbarth, B. Röder and G. Schnurpfeil, *J. Porphyrins Phthalocyanines*, 1998, **2**, 145.
29 J. M. Tsay, M. Trzoss, L. Shi, X. Kong, M. Selke, M. E. Jung and S. Weiss, *J. Am. Chem. Soc.*, 2007, **129**, 6865.
30 H. Shinohara, O. Tsaryova, G. Schnurpfeil and D. Wöhrle, *J. Photochem. Photobiol., A*, 2006, **184**, 50.
31 A. P. Losev, I. M. Byteva and G. P. Gurinovich, *Chem. Phys. Lett.*, 1988, **143**, 127.
32 C. Marti, O. Jürgens, O. Cuenca, M. Casals and S. Nonell, *J. Photochem. Photobiol., A*, 1996, **97**, 11.
33 X. Zarate, E. Schott, T. Gomez and R. J. Arratia-Pérez, *Phys. Chem. A*, 2013, **117**, 430.
34 C. A. Caro, F. Bedioui, M. A. Paez, G. I. Cardenas-Jiron and J. H. Zagal, *J. Electrochem. Soc.*, 2004, **151**, E32.
35 A. B. P. Lever, E. R. Milaeva and G. Speier, in *Phthalocyanine: Properties and Applications*, ed. A. B. P. Lever and C. C. Leznoff, VCH, New York, 1993, vol. 3, pp. 1–69.
36 A. R. Özkaya, A. G. Gürek, A. Gül and Ö. Bekaroğlu, *Polyhedron*, 1997, **16**, 1877.
37 Y. Zhang, P. Ma, P. Zhu, X. Zhang, Y. Gao, D. Qi, Y. Bian, N. Kobayashi and J. Jiang, *J. Mater. Chem.*, 2011, **21**, 6515.
38 R. Li, X. Zhang, P. Zhu, D. K. P. Ng, N. Kobayashi and J. Jiang, *Inorg. Chem.*, 2006, **45**, 2327.
39 (*a*) J. I. Brauman and L. K. Blair, *J. Am. Chem. Soc.*, 1970, **92**, 5986; (*b*) K. Naka, T. Uemura and Y. Chujo, *Macromolecules*, 2002, **35**, 3539.
40 (*a*) T. B. McMahon and P. Kebarle, *J. Am. Chem. Soc.*, 1977, **99**, 2222; (*b*) J. M. Karty, Y. Wu and J. I. Brauman, *J. Am. Chem. Soc.*, 2001, **123**, 9800.
41 X. Wang, Y. Zhang, X. Sun, Y. Bian, C. Ma and J. Jiang, *Inorg. Chem.*, 2007, **46**, 7136.
42 B. Tylleman, G. Gbabode, C. Amato, C. Buess-Herman, V. Lemaur, J. Cornil, R. G. Aspe, Y. H. Geerts and S. Sergeyev, *Chem. Mater.*, 2009, **21**, 2789.
43 M. Ishida, S. W. Park, D. Hwang, Y. B. Koo, J. L. Sessler, D. Y. Kim and D. Kim, *J. Phys. Chem. C*, 2011, **115**, 19343.

44 L. Yang, L. Guo, Q. Chen, H. Sun, H. Yan, Q. Zeng, X. Zhang, X. Pan and S. Dai, *J. Mol. Graphics Modell.*, 2012, **38**, 82.
45 M. Thelakkat and H.-W. Schmidt, *Adv. Mater.*, 1998, **10**, 219.
46 (*a*) N. Zharnikova, N. Usol'tseva, E. Kudrik and M. Thelakkat, *J. Mater. Chem.*, 2008, **19**, 3161; (*b*) L. Zhu, H. Tang, Y. Harima, Y. Kunugi, K. Yamashita, J. Ohshita and A. Kunai, *Thin Solid Films*, 2001, **396**, 213.
47 A. G. Gürek and Ö. Bekaroglu, *J. Chem. Soc., Dalton Trans.: Inorg. Chem.*, 1994, **9**, 1419.
48 P. M. Burnham, M. J. Cook, L. A. Gerrard, M. J. Heeney and D. L. Hughes, *Chem. Commun.*, 2003, 2064.
49 D. Aydın Tekdaş, U. Kumru, A. G. Gürek, M. Durmuş, V. Ahsen and F. Dumoulin, *Tetrahedron Lett.*, 2012, **53**, 5227.
50 T. Muto, M. Kimura, K. Hanabusa and H. Shirai, *Tetrahedron Lett.*, 1999, **40**, 3199.
51 A. T. R. Williams, S. A. Winfield and J. N. Miller, *Analyst*, 1983, **108**, 1067.
52 P. Jacques and A. M. Braun, *Helv. Chim. Acta*, 1981, **64**, 1800.
53 J. M. Soler, E. Artacho, J. D. Gale, A. García, J. Junquera, P. Ordejón and D. Sánchez-Portal, *J. Phys.: Condens. Matter*, 2002, **14**, 2745.
54 J. P. Perdew, K. Burke and M. Ernzerhof, *Phys. Rev. Lett.*, 1996, **77**, 3865.
55 N. Troullier and J. L. Martins, *Phys. Rev. B: Condens. Matter*, 1991, **43**, 1993.
56 L. Kleinman and D. M. Bylander, *Phys. Rev. Lett.*, 1982, **48**, 1425.